RI

AD-A249 662

E

1. AGENCY USE ON	3-17-92	Final 8/1/88 - 12/31/91

4. TITLE AND SUBTITLE

Focused Ion Beam Implantation

5. FUNDING NUMBERS

DAAL03-88-K-0108

6. AUTHOR(S)

Dr. John Melngailis

7. PERFORMING ORGANIZATION NAME(S) AND ADDRESS(ES)

Research Laboratory of Electronics
Massachusetts Institute of Technology
77 Massachusetts Avenue
Cambridge, MA 02139

8. PERFORMING ORGANIZATION REPORT NUMBER

9. SPONSORING/MONITORING AGENCY NAME(S) AND ADDRESS(ES)

U.S. Army Research Office
P.O. Box 12211
Research Triangle Park, NC 27709-2211

10. SPONSORING/MONITORING AGENCY REPORT NUMBER

ARO 26051.5-EL

11. SUPPLEMENTARY NOTES

The view, opinions and/or findings contained in this report are those of the author(s) and should not be construed as an official Department of the Army position, policy, or decision, unless so designated by other documentation.

12a. DISTRIBUTION/AVAILABILITY STATEMENT

Approved for public release; distribution unlimited.

12b. DISTRIBUTION CODE

13. ABSTRACT *(Maximum 200 words)*

The goals of this research program were to develop devices fabricated by focused ion beam implantation, such as tunable Gunn diodes, GaAs MESFET's, silicon MOSFET's or other novel devices, and to advance the focused ion beam technology. All the goals were reached and are reported in this report.

14. SUBJECT TERMS

Device Fabrication, Ion Beams, Gunn Diodes, MESFETS, MOSFETS
Ion Beam Technology

15. NUMBER OF PAGES 20

16. PRICE CODE

17. SECURITY CLASSIFICATION OF REPORT	18. SECURITY CLASSIFICATION OF THIS PAGE	19. SECURITY CLASSIFICATION OF ABSTRACT	20. LIMITATION OF ABSTRACT
UNCLASSIFIED	UNCLASSIFIED	UNCLASSIFIED	UL

Final Report

on

Contract no. DAAL 03-88-K-0108

"Focused Ion Beam Implantation"

by

John Melngailis

From 8/1/88 to 12/31/91

The goals of this research program were to develop devices fabricated by focused ion beam implantation, such as tunable Gunn diodes, GaAs MESFET's, silicon MOSFET's or other novel devices, and to advance the focused ion beam technology. We have succeeded in all of these goals as will be reported below.

1. Technology improvements

In order to reliably and efficiently fabricate the devices made during this program of research a number of improvements in the focused ion beam technology were needed. Assuming that the focused ion beam column delivers a beam of the desired ions of the diameter needed between 0.05 and 0.5 μm and at the desired energy the remaining challenge is to blank and deflect the beam with the required precision so as to deliver the required dose to each part of the surface. In most cases these implants have to be located precisely with respect to existing structures on the wafer. To achieve this we have developed procedures for precisely deflecting the ion beam and for aligning the written structures with respect to alignment marks on the wafer. The sample stage position is measured by a laser interferometer to a precision of $\pm$ 0.01 μm. This permits the deflection fields of the ion beam to be stitched together. By measuring the positions of alignment marks, viewed in the scanning ion microscope mode, we have been able to develop a coordinate rotation and calibration matrix which accounts for the fact that the x-y axis defined by the existing pattern on the wafer is not aligned to the x-y axis of the sample stage travel nor to the x-y axis of the beam deflection. The end result is that we have been able to verify a placement capability of $\pm$ 0.1 μm. This was done by writing vernier structures in PMMA aligned to vernier structures previously fabricated on the sample in both the x and y axis. Some of this work is described in the paper abstract in Appendix A.

In addition we have learned how to operate the ion source more reliability by moving the beam defining aperture farther from the source and by operating some of the sources (such as Au Si Be) at higher extraction currents. Overall we have achieved more reliable operation and an increased throughput on our machine.

One of the results of the effective operation of the machine was the writing of x-ray lithography masks (see Appendix A-1) which were used to observe resonant tunneling in surface structured quantum wells (see Appendix A-2). The lithography was carried out using Be^{++} ions at 280 keV. 0.05 μm minimum width lines were exposed in 0.3 μm thick PMMA and plated up with gold to a thickness of 0.25 μm. The gold lines were well defined with smooth vertical sidewalls (Appendix A-1).

2. Fundamentals of focused ion beam implantation

We have addressed two aspects of focused ion beam implantation: the dose rate effects due to the high instantaneous current density and the limited straggle due to channeling.

a) Dose rate effects. Due to the high instantaneous current density of focused ion beam implantation one might expect that the amount of damage and carrier activation may be different for focused ion beam and broad beam implantation. Accordingly we implanted identical areas with a conventional implanter and with a focused ion beam. A comparison of the characteristics of the areas revealed some differences.

We measured directly the distribution of the implanted Si in GaAs for both on-axis and off-axis and for both focused and broad beams. In both cases the focused ion beam implants showed less penetration in the tails although the peaks of the implants were at the same depth. Based on some

other observations, which we will describe shortly, this lowered tail penetration can be attributed to increased surface amorphization in the case of the focused ion beams.

In addition we have measured the sheet resistivity and Hall sheet concentration as a function of dose for the different cases. Above a dose of $3x10^{13}$ ions/cm^2 (Si ions at 140 and 280 keV in GaAs) the sheet resistance and the carrier density saturate in the case of broad beam implantation. In the case of focused ion beam implantation the sheet resistance actually decreases with increasing dose above $3x10^{13}$ ions/cm^2 and the sheet electron concentration drops. Apparently even after annealing the increased damage in the focused ion beam case impedes carrier activation. We have also confirmed this be measuring the carrier concentration as a function of depth by Hall sectioning, i.e. etching off a known thickness and then repeating the Hall measurements. In the case of focused ion beam implants at $1x10^{14}$ there is actually a layer on the surface where no activation is produced. These considerations are important in designing of the implantation schedules for various devices. In practice one can also avoid some of these effects by scanning the focused ion beam rapidly over the surface to be implanted. This will lower the instantaneous current density. In addition, devices need to be designed with ion doses less than $3x10^{13}$/cm^2 in which case focused and broad beam implants are identical. These measurements were needed to implant the tunable Gunn diodes. The abstract of a paper on this is in Appendix B.

b) Limited Straggle

The resolution of focused ion beam implanted patterns is determined by the diameter of the ion beam, by the lateral straggle, and by any diffusion during annealing. In most cases, particularly for light ions the straggle is the most important factor.

Recent results in the literature suggest that ions implanted along the crystal axis straggle laterally less and penetrate deeper than previously expected. This had been observed so far only by cathodo-luminescence in quantum wells. We have measured the lateral straggle by direct electrical means. Gratings were implanted using Be^{++} ions at 260 keV with periods from 0.04 μm to 3 μm both parallel and perpendicular to the direction of current flow. In the parallel case the implant is along the (100) axis into an n-type epitaxial layer and converts the material into an insulator in the implanted stripes. The period at which these stripes join and completely cut off the conduction depends on the initial beam diameter and the lateral straggle. The surprising result is that even for periods as low as 0.1 μm the conductivity is still modulated by the grating.

In the perpendicular case the gratings are implanted into semiinsulating GaAs between two existing p-type contact regions and annealed. Both on-axis and off-axis implants were carried out. In off-axis material the lateral straggle was found to be 50 to 90 nm larger depending on the dose. Monte-Carlo theory would have predicted 450 nm of straggle. In neither on-nor off-axis implants did the width of the lines reach this theoretical prediction.

The fact that the straggle is limited is important for applications, such as quantum devices, where the spreading of implanted species can be detrimental to the operation. (This work will be published in Applied Physics letters, abstract is attached in Appendix C.)

We have also attempted to measure the straggle for both on-axis and off-axis implantation of boron in Si. The experiments are similar to those described above for GaAs. The masks have been designed and two sets of wafers (i.e. on-and off-axis) have been implanted.

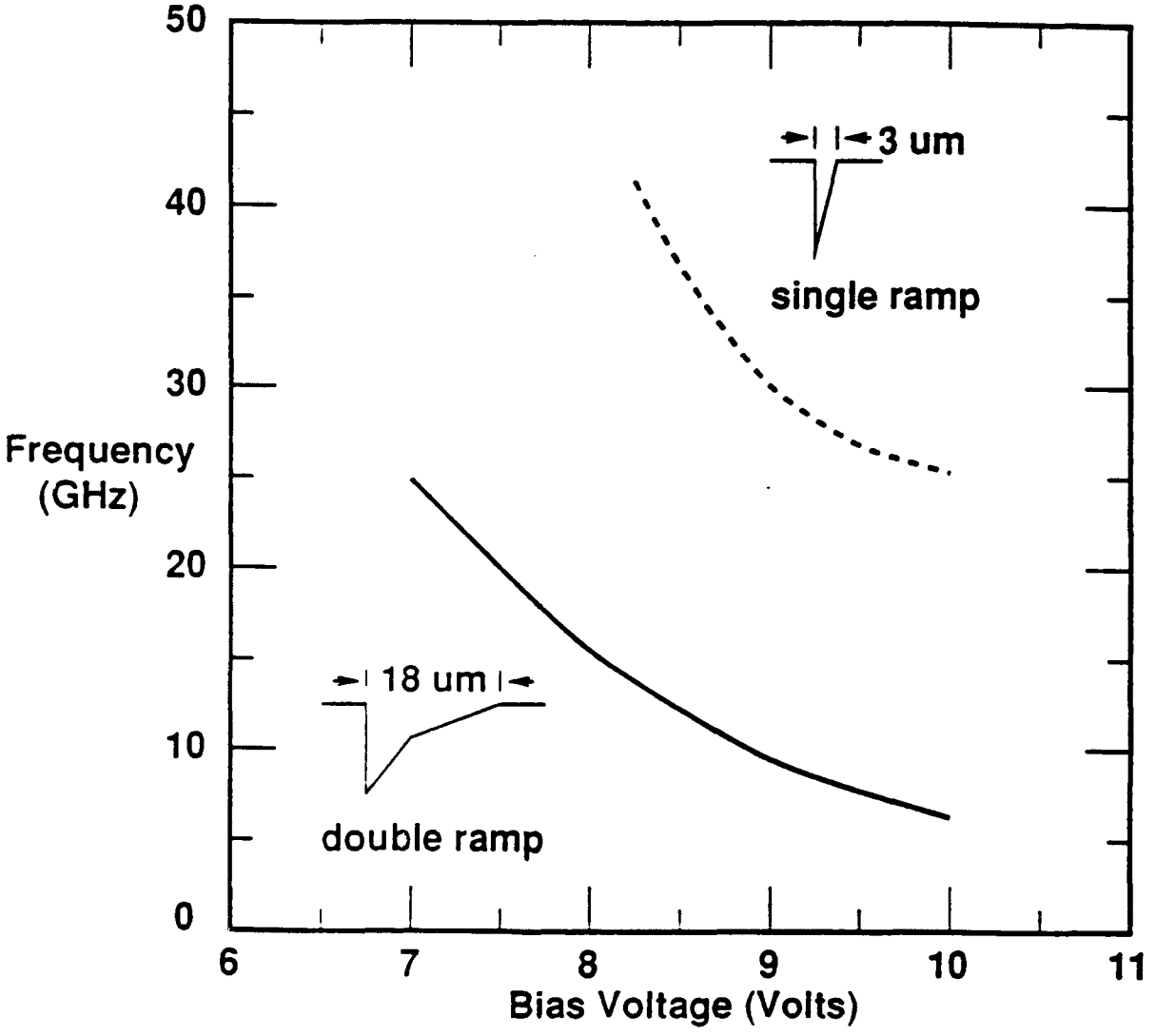

Fig. 1 Frequency versus bias voltage for two tunable Gunn diodes in gallium arsenide. These diodes were fabricated with lateral doping gradients over the range 5×10^{12} to 1.3×10^{13} ions/cm^2. The two insets schematically show the doping gradients.

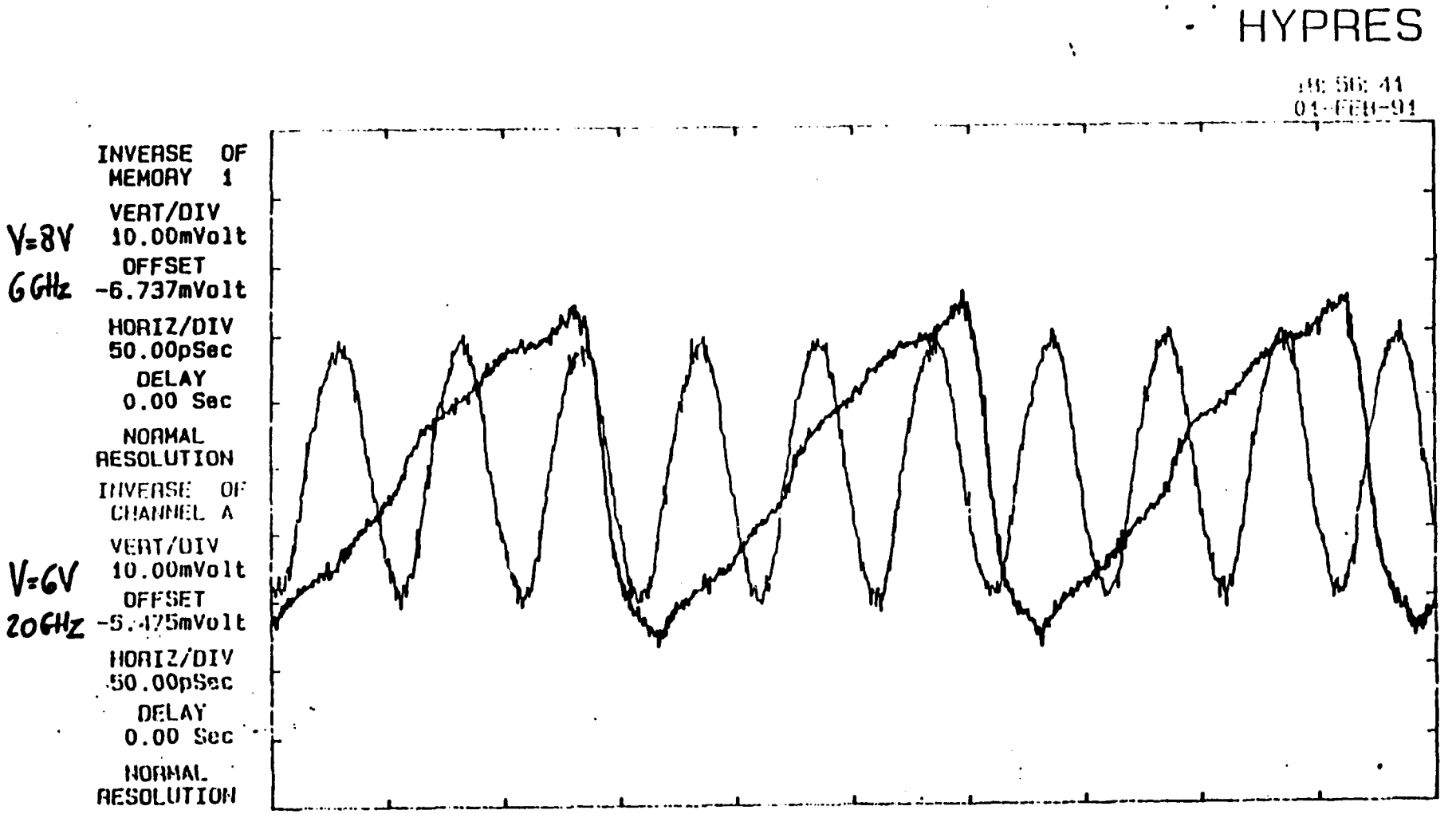

Fig. 2 The waveform obtained from a tunable Gunn diode at 6 GHz and at 20 GHz as measured on a Hypress oscilloscope. The horizontal scale is 50 psec/div. At 6 GHz a clearly triangular waveform is observed in qualitative agreement with simulation. (Fig. 3).

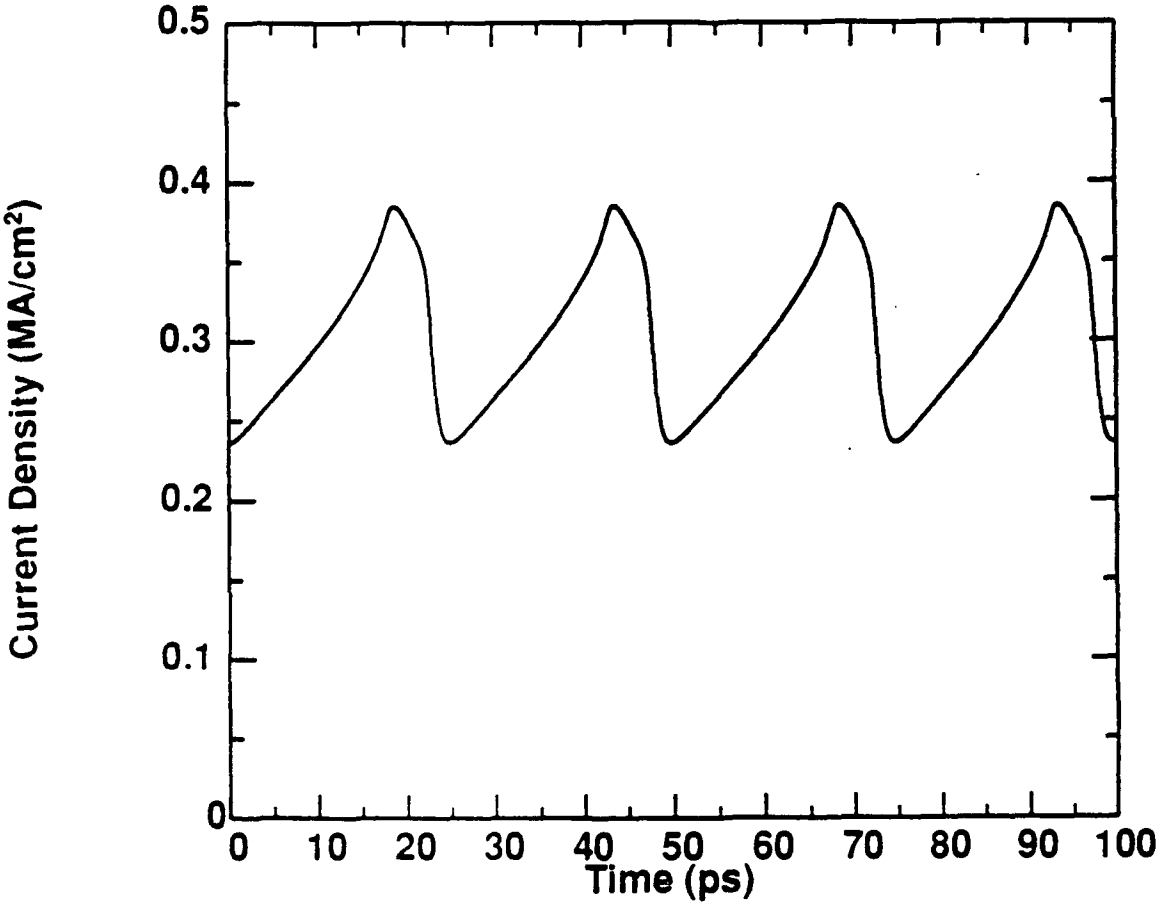

Fig. 3 Graded device, Boltzmann simulation, 2V bias: Simulated current waveform.

3. Devices

Using the improved technology and the increased understanding of the focused ion beam implantation process we have fabricated a number of devices some with unique or much improved performance, including tunable Gunn diodes, MOSFET's and MESFET's with improved characteristics, and CCD's with 15 times higher clocking speeds.

a) Tunable Gunn diodes. These devices were first conceived and demonstrated under our previous contact. (See Appendix D). If a gradient of doping is implanted between two contacts so that the carrier density increases gradually from contact to contact, say, from a level of 2.3×10^{17} to $4 \times 10^{17}/cm^3$ achieved by implanting doses between 1 & $3 \times 10^{13}/cm^2$, then the oscillation frequency will be a function of the bias. The Gunn domain is launched from the point where the carrier density is lowest and the electric field is highest and travels toward the region of higher carrier density. As this happens the field in the low density end is rising. When it passes a threshold value a new domain is launched and the previous domain dies out. The domain velocity is of order 10^7 cm/sec, and device oscillation up to 42 GHz has been observed for the shortest (3 μm) devices. The frequency responses of two Gunn diodes are shown in Fig. 1.

The waveform of the Gunn oscillations has been recorded using a special high-speed oscilloscope, and shows a triangular form at the lower frequency of 6 GHz. At 20 GHz the higher frequency components of the signal are apparently attenuated so that the observed wave form is more nearly sinusoidal, see Fig. 2. The performance of the Gunn diodes has been extensively simulated using a Boltzman equation formulation, programmed for the Cray computer. The tuning characteristics and the triangular waveform Fig. 3 are predicted. This is a large part of the Ph.D. theses of H.

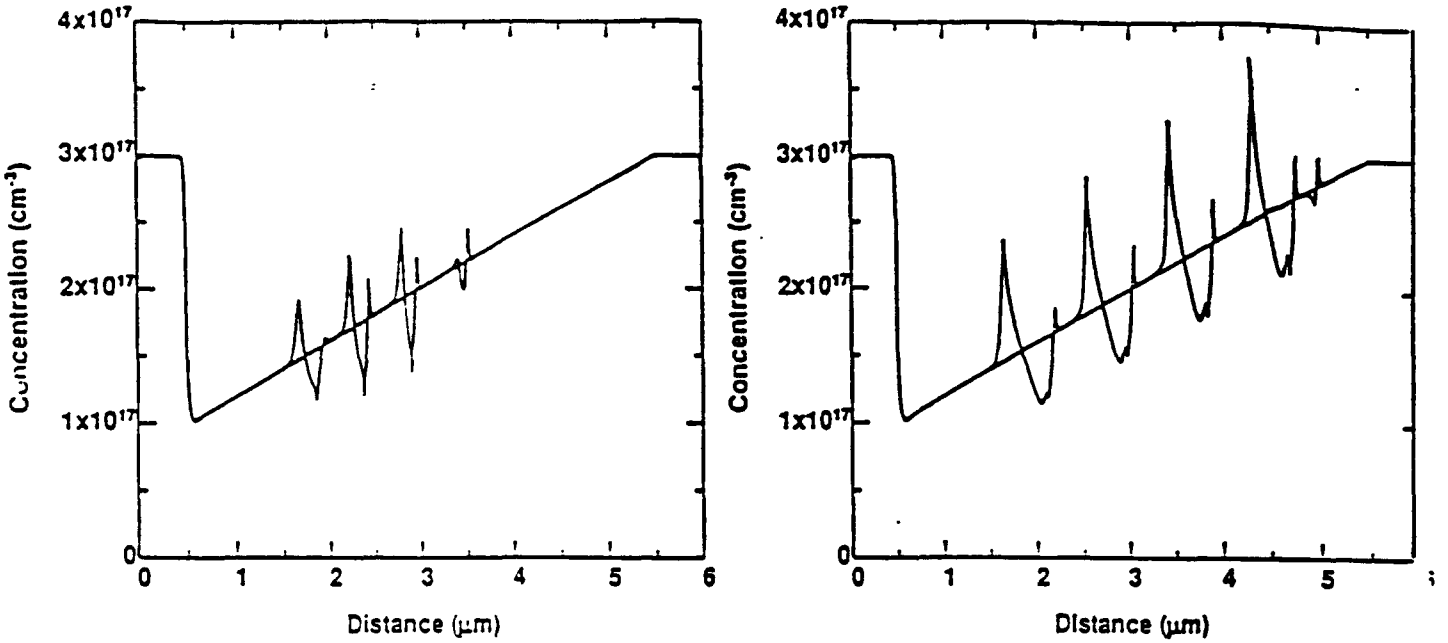

Fig. 4 Simulated electron concentration profiles vs. lateral position at successive time intervals during domain propagation. Left) bias = 2 V, freq = 40 GHz, Δt = 6 psec Right) bias = 6 V, freq = 25 GHz, Δt = 12 psec

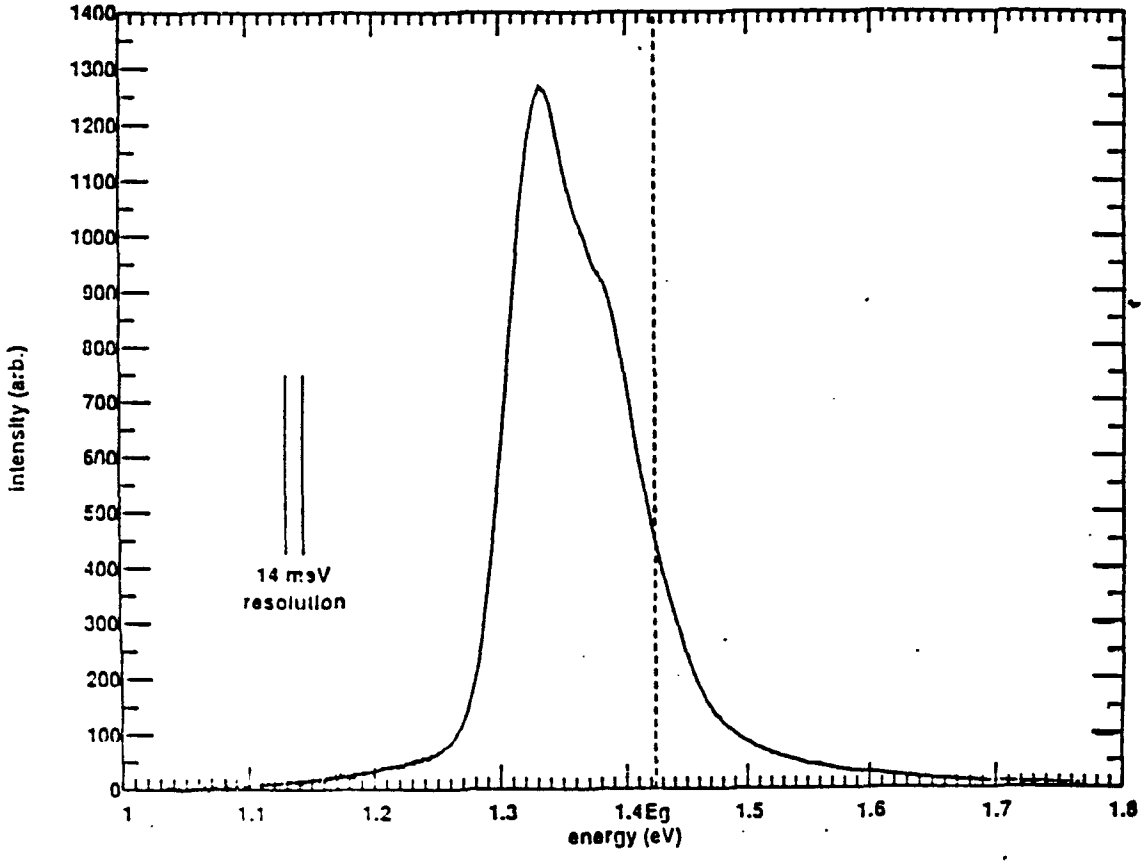

Fig. 5 The spectrum of radiation emitted by the region where the Gunn domain is propagating.

Lezec and C. Musil (H. Lezec will defend his thesis in March 1992.) An abstract of a paper submitted to the Device Research Conference is in Appendix E. One of the quantities calculated in the simulation is the charge density in the Gunn domain. This is shown in Fig. 4 at various picosec time intervals as it propagates up the background charge density ramp.

During one of the experiments, as the test probes were being positioned on a tunable Gunn diode under the microscope, light emission was observed coming out of the area where the Gunn domain propagates. We measured the spectrum of this light and found it to peak below the band gap with a tail extending into the visible spectrum. Fig. 5. That the light comes only from the region where the Gunn domain propagates was verified by observing that the rectangular bright area changes size as the bias and hence the frequency and the length over which the domain propagates is changed. Our simulations predict that in the Gunn domain the electric field has a value up to 140 kV/cm. We believe that the light emission is due to avalanche breakdown and the fact that it is shifted below the bandgap is due to local heating by the Gunn domain.

b) Applications of tunable Gunn diodes

We have explored the practical applications of the tunable Gunn diodes in collaboration with researchers at Mitre Corp. and at M/A Com. The devices were tested in various ways, for example, as components in injection locked voltage controlled oscillators or dielectric resonator oscillators. In general the tunable Gunn diodes provide a simple low cost generic swept frequency source with numerous potential applications. One of the most immediate is for built in testing of microwave systems. This would eliminate the need in many cases of removing circuit elements from their systems for the testing of their frequency response. Alternatively one can envisage high

frequency test probes with the high frequency source built into the tip of the probe. Some of these results were reported in a paper given at the 1991 MTT Symposium. Appendix F.

c) GaAs MESFET's

GaAs MESFET's have been built with a gradient of doping in the channel region. The gate lengths were between 0.5 and 5 μm. These gates were fabricated by focused ion beam lithography with a SiN layer under the PMMA resist to prevent ion damage to the channel. A 20% higher transconductance was achieved. The unity short-circuit current-gain frequency f_t, which is inversely proportional to the transit time of carriers through the control region, is considerably increased by the presence of a gradient. For 2 μm-gate length F_t = 3 GHz with no gradient to 8.4 GHz with a gradient. For 1 μm-gate length the improvement was from F_t = 6.8 to 10.4 GHz. The devices have been modelled by the same program which was used for the Gunn domains. In fact, the MESFET's frequently exhibit stationary Gunn domains.

d) MOSFET's on Si

NMOS and PMOS transistors in Si were implanted with various doping profiles in the channels. In all, over 2000 variations were produced. Both B and As ions were used at various energies. The implants were aligned to $\pm$ 0.1 μm to the features fabricated by standard optical lithography on the surface. This work illustrates the utility of the focused ion beam as a prototyping tool. To fabricate 2000 variations in the channel doping by conventional means would be unthinkable.

Line implants along the source-gate boundary (e.g. a B^+ implant in an NMOS device) were found to increase the transconductance by 20% and lead to a large decrease of output conductance resulting in an increase in open

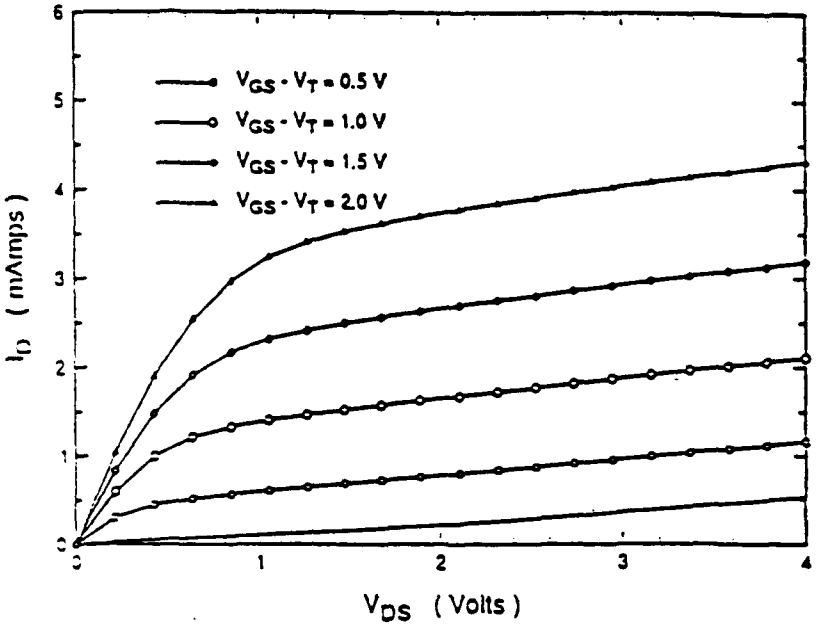

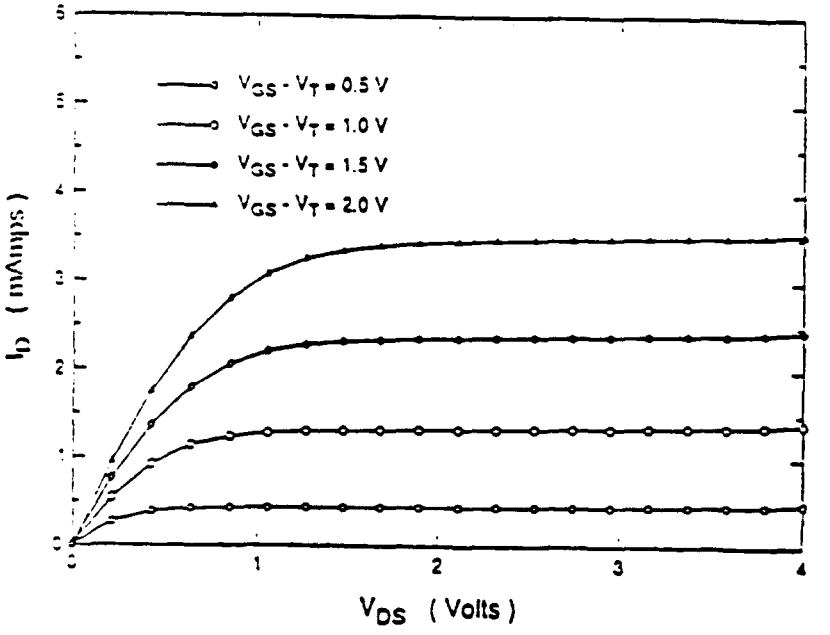

Fig. 6 (a)The measured drain current I_D vs. drain source voltage V_{DS} for a 1.2 μm gate length MOSFET for various gate voltage V_{GS}.

(b)The I_D vs. V_{DS} characteristics for the same device with an FIB implant along the source. Note the almost zero slope of the curves at higher V_{DS} implying a high output conductance and a 20 times higher open circuit gain.

circuit gain of a factor of 20 (see Fig. 6). Similar behavior was found for PMOS transistors implanted with As. The flexibility of the focused ion beam permitted the position of the line implant and its dose to be varied so that the optimum conditions were determined.

e) Charge Coupled Devices (CCD's)

CCD's were fabricated with doping gradients in the channels in the direction of current flow. These were buried channel device with 26 μm long channels. In long channel CCD's, such as used in imaging devices, the clocking speed is limited by the ability of residual charge to diffuse out of the channel. A doping gradient creates a built in electric field which pushes the charge out faster. Such CCD's were simulated, designed and built in collaboration with Lincoln Laboratory. CCD's with no doping gradient were found to have a maximum clocking frequency of 2.5 MHz while those with the doping gradient were found to clock 15 times faster, i.e. at 41 MHz. The doping gradient was very slight, corresponding to a dose variation from 0 to 1.5×10^{11} ions/cm^2 over 26 μm. In addition, high resolution is not needed so that a higher-current, larger-diameter beam can be used. This implies that writing time is very short, and that this technique could be used in practice. See papers Appendix G and H.

Personnel Supported

H. Lezec	Graduate student EE&CS, Ph.D. EE&CS (June 1992, expected)
C. Musil	Graduate student Physics
J. Murguia	Graduate student EE&CS (Ph.D. EE&CS 1991)
D. Vignaud	Visiting Scientist, 1991 (Partial Research Support Only)
A. Shimase	Visiting Scientist - 1991 (Partial Research Support Only)
S. Etchin	Research Engineer from 4/15/91
M. Shepard	Research Engineerr (up to 6/1/91)
D.A. Antoniadis	Professor EE&CSS (Co-Pi)
J. Melngailis	Senior Research Scientist RLE & EE&CS (Co-Pi)

Appendix A

Merging focused ion beam patterning and optical lithography in device and circuit fabrication

James E. Murguia, Christian R. Musil, Mark I. Shepard, Henri Lezec, Dimitri A. Antoniadis, and John Melngailis

Room 39-659, Department of Electrical Engineering and Computer Science, Massachusetts Institute of Technology, Cambridge, Massachusetts 02139

(Received 29 May 1990; accepted 31 July 1990)

Combining optical lithography and focused ion beam (FIB) patterning in direct-write device and circuit fabrication by generating large features optically and small features with the FIB can significantly reduce beam writing time. Our approach to FIB pattern definition is ideally suited for alignment to optically patterned features and takes full advantage of the lithographic and implantation capabilities of the FIB. Optical and FIB patterns are designed simultaneously in the very large scale integrated layout tool MAGIC, [MAGIC, Report No. UCB/CSD 85/225 University of California, Berkley (March 1985)]. We have developed a software package MAGTOFIB [James E. Murguia, Christian Musil, Mark Shepard, Sasan Zamani, MAGTOFIB, Massachusetts Institute of Technology (1989)] which takes its input from the MAGIC data file and converts it to FIB stage and beam commands. The FIB is aligned by operating in scanning ion microscope mode and finding the centroid of an optically produced die alignment mark. Since the coordinate systems of a typical optical reticle, stepper, and of the FIB are, in general, nonorthogonal and rotated with respect to the wafer, the alignment error increases as one moves away from the alignment point. To place features 1 cm apart to an accuracy of 0.1 μm, calibration must be better than one part in 10^5. This precision is achieved with a linear transformation calculated from three alignment crosses on the pattern perimeter which transform computer aided design layout coordinates into wafer coordinates. The transformation is calculated once per wafer. The patterning tools have been demonstrated using three types of alignment marks and two resists, on a variety of devices, as well as x-ray masks. The alignment accuracy is ± 0.1 μm. In addition, we report a process to combine optical and FIB lithography on the same layer using the same positive UV resist (KTI 820) as a negative FIB resist.

I. INTRODUCTION

In this article we propose a scheme for integrating a focused ion beam (FIB), for lithography and maskless implantation, into a semiconductor device and circuit processing line. Our approach allows the strengths of FIB and of optical lithography to complement each other. By merging the two lithographic techniques, large features can be generated optically, and small features with the FIB, significantly reducing FIB writing time, or conversely, making ultrafine features available in an optical process.[1] We begin with a short description of the column, emphasizing the interaction of the beam deflection electronics with the motion of the mechanical stage.

The electronic deflection of the beam takes place at two locations in the column. At the top of the column, a blanker shutters the beam by applying a 40 V potential perpendicular to the ion beam. A deflecting octopole is located between the final lens and the sample. The octopole steers the beam within the deflection field. The blanker and the deflection octopole are controlled by a bit slice processor which is computer programmed. The exact location of the stage ($\pm$ 10 nm) is measured with a laser interferometer.

The deflection field has two components, the vector field and the raster field. The vector field contains the raster field. A vector offset is applied to the raster field to pattern a trapezoid. Ten nanometer placement accuracy on a 0.1-μm beam with 50% beam overlap limits the maximum vector and raster field sizes to 163 and 12.6 μm, respectively. Features larger than the raster field are broken up into several raster fields, and features larger than the vector field are broken up into several vector fields with stage motion.

FIB semiconductor processing technology is unique in that it can be used to expose resist and to implant impurities. Merging this technology into an optical process without sacrificing FIB system capabilities requires some modification to the existing very large scale integrated (VLSI) computer aided design (CAD) tool suite. To this end, we have developed a filtering program MAGTOFIB which translates layout information from the VLSI circuit layout tool MAGIC into commands understood by the FIB. These tools allow the definition of FIB lithography and implantation to proceed simultaneously with optical mask design.

In Sec. II–IV we describe the tool MAGTOFIB, the technique used to align the FIB to the optical mask set, and the alignment marks, respectively. Section V verifies alignment, and Sec. VI describes a novel process for combining optical and FIB lithography in the same process step.

II. SIMULTANEOUS FIB AND OPTICAL PATTERN DEFINITION

Two display issues arise when merging FIB and optical CAD layouts. First, the scale differences between a FIB pattern and a UV pattern suggest the minimum feature size on

 0734-211X/90/061374-06$01.00

Sub-100-nm x-ray mask technology using focused-ion-beam lithography

W. Chu, A. Yen, K. Ismail, M. I. Shepard, H. J. Lezec, C. R. Musil, J. Melngailis, Y.-C. Ku, J. M. Carter, and Henry I. Smith
Massachusetts Institute of Technology, Cambridge, Massachusetts 02139

(Received 8 June 1989; accepted 7 July 1989)

In the past, nearly all x-ray nanolithography (i.e., sub-100-nm linewidths) employed the C_K x-ray line at 4.5 nm. This, in turn, necessitated near-zero gaps (to avoid diffraction) and carbonaceous masks (e.g., polyimide, which is subject to distortion). In order to use x-ray replication in the fabrication of multilevel devices and circuits that cover large areas (~a few cm^2) and have feature sizes well below 100 nm, we have turned to the Cu_L line at 1.3 nm. Masks consist of 1–1.5 μm thick Si or Si_3N_4 membranes and Au absorber patterns, 200 nm thick, which provide 10 db contrast. Focused-ion-beam-lithography (FIBL) with Be^{++} ions at 280 keV was used to produce quantum-effect-device patterns with minimum linewidths of ~50 nm. These were replicated using the Cu_L line, indicating that photoelectrons are not a serious problem. The FIBL process [exposure of 300 nm-thick polymethylmethacrylate (PMMA), followed by Au electroplating] is high yield and much simpler than a trilevel electron-beam-lithography process designed to give comparable results. This is the first time FIBL has been used to make x-ray masks at sub-100-nm linewidths. Along with the device patterns, linear-zone-plate alignment marks were also written on the masks, to be aligned to corresponding marks on the substrate via an optical alignment scheme.

I. INTRODUCTION

X-ray lithography has been used in the fabrication of a wide range of sub-100-nm-linewidth structures and devices, most recently, metal–oxide-semiconductor field effect transistors (MOSFETs),[1,2] quantum wires,[3,4] and lateral-surface superlattices.[5] In all but a few examples of such work the carbon K (C_K) x-ray line at 4.5 nm was used. The C_K line is attractive for nanolithography (i.e., sub-100-nm features) for two reasons: (1) a contrast of 10 db can be achieved in films of Au or W only 80 or 63 nm thick, respectively; (2) any loss of resolution due to photoelectrons should be minimal since their effective range is expected to be ~5 nm. On the other hand, use of the C_K line carries two significant disadvantages: (i) diffraction is proportionally greater than if a shorter wavelength, such as Cu_L (1.33 nm), were used; (ii) only carbonaceous materials provide sufficient x-ray transmission for use as a mask membrane. Diamond or some other form of hard, transparent carbon might be an ideal membrane material for use with the C_K line, but, since these materials are not readily available, we have used polyimide membranes 1–2 μm thick. Polyimide is suitable only for single level patterning because it is subject to distortion, and tends to wrinkle with usage. Also, breakage is common. Thus, in order to use x-ray lithography in the fabrication of devices and circuits that require multilevel alignment, cover large areas (~a few cm^2), and have feature sizes below 100 nm, an x-ray wavelength between 1 and 1.5 nm appears to be essential at the present time. In this wavelength range, which is the same as the range for commercial scale lithography of 0.25–1.0 μm linewidths,[6,7] inorganic membrane materials, such as Si, Si_3N_4, SiC, etc., are available. Masks made from these materials can be free of distortion if the stress in the absorber is sufficiently low.[8] They are also unusually strong and breakage resistant.

If one is restricted to electron-bombardment sources, the most suitable x-ray emission line in the 1 to 1.5 nm range is the Cu_L at 1.33 nm.[9–11] This line permits the use of a pi-phase-shifting mask,[12] and it appears that the attendant enhancement of process latitude should permit 50 nm linewidths to be replicated at 5 μm mask-to-substrate gaps.[11–13]

The objectives of the study reported here were to develop an inorganic membrane mask technology suitable for sub-100-nm x-ray lithography, to pattern and electroplate gold absorber with the 50 nm linewidth interdigital electrode patterns of a novel quantum-effect device [the planar resonant tunneling field-effect transistor (PRESTFET)],[14] to optically align the resulting mask with respect to alignment marks on a substrate, and to demonstrate by this sequence the utility of the Cu_L line in x-ray nanolithography.

II. MASK FABRICATION

Most of our work has been done with Si-rich Si_3N_4 membranes.[15] If they are initially free of defects such as pinholes, they are extremely strong and durable. For example, a 20 mm diameter, Si-rich Si_3N_4 membrane, 1.4 μm thick, can sustain a full atmosphere of pressure differential, deflecting ~700 μm, but not breaking. Such membranes do not break in ordinary usage unless struck directly with a sharply pointed object. They can be brought repeatedly into contact with a substrate, with no apparent damage.

At the Cu_L line, the absorption of Au is 50 db/μm. To get a 10 db contrast, 200 nm absorber thickness is required, 2.5 times more than with the C_K line. Since the pattern of interest (the PRESTFET) has lines and spaces of 50 nm, electroplating is the preferred method. Earlier, we described a trilevel process for making x-ray masks by electron-beam (e-beam) lithography that consisted of exposing and deve-

Resonant tunneling across and mobility modulation along surface-structured quantum wells

K. Ismail[a] and W. Chu
Department of Electrical Engineering and Computer Science, Massachusetts Institute of Technology, Cambridge, Massachusetts 02139

R. T. Tiberio
National Nanofabrication Facility, Cornell University, Ithaca, New York 14853-5403

A. Yen, H. J. Lezec, M. I. Shepard, C. R. Musil, J. Melngailis, D. A. Antoniadis, and Henry I. Smith
Department of Electrical Engineering and Computer Science, Massachusetts Institute of Technology, Cambridge, Massachusetts 02139

(Received 31 May 1989; accepted 18 July 1989)

We present results of fabrication and transport measurements on surface-structured quantum wells. The structures are fabricated on GaAs/AlGaAs modulation-doped layers. Three different devices are examined: the grid-gate lateral-surface-superlattice, the planar-resonant-tunneling field-effect transistor, and the multiple parallel quantum wires. In the first two structures, transport is perpendicular to the field-induced potential barriers. At 4.2 K, we observed evidence for resonant tunneling in both types of devices. In the third type of structure, transport is through isolated quantum wires parallel to the barriers. The presence of one-dimensional energy subbands, and mobility modulation, above and below the two-dimensional value, were observed.

I. INTRODUCTION

With the advent in sub-100 nm lithography and band gap engineering techniques, structures can be fabricated in which the wave nature of the electrons is manifested in interference and diffraction effects. We have focused on *planar* nanostructures built on GaAs/AlGaAs modulation-doped layers, where low temperature electrons can have a mean free path and a coherence length of the order of micrometers. As a variation from the ordinary single-gate MODFET, we have studied three types of devices: the lateral-surface-superlattice (LSSL), the planar-resonant-tunneling field-effect transistor (PRESTFET), and multiple-parallel quantum wires (MPQW). Although the underlying physical principles in the three types of devices are different, they have one thing in common: the potential distribution in a two-dimensional electron gas (2DEG) is perturbed by an externally-controlled field effect. In all three structures, either single or multiple quantum wells are induced at the surface, and due to the additional confinement, zero or one-dimensional quantized levels are created. The electron transport properties across and along those quantum wells is investigated.

II. DEVICE STRUCTURE AND FABRICATION

The periodic structures in the LSSL devices and the MPQW were produced using x-ray nanolithography, and the modulation-doped layers were grown by MBE, as previously discussed.[1] Four-probe Van der Pauw measurements gave a mobility of 300,000 $cm^2/V\,s$ at 4 K. The gate structures used in the PRESTFET device were exposed using electron-beam (e-beam) and focused-ion-beam (FIB) nanolithography. In the FIB system, Be^{++} ions at an energy of 280 keV were used to expose 120 nm thick polymethylmethacrylate (PMMA). The range of the Be species at this energy is expected to be $\sim 1\ \mu m$ in PMMA and $0.7\ \mu m$ in GaAs. Exposure conditions were chosen to achieve the highest possible resolution. Lines having a minimum width of 50 nm could be delineated. The e-beam system was a JEOL JBX5D11 located at the National Nanofabrication Facility. Electrons at an energy of 50 keV were used, and a minimum linewidth of 55 nm was achieved.

We have previously reported on the fabrication and measurements of grating-gate and grid-gate LSSL devices.[1-3] In the most recent improvement of the process, we generated x-ray masks that had a two-dimensional array of Au absorber squares. Using those masks for exposure, combined with evaporation and liftoff, metal grids were achieved in a single step. The linewidth of the Schottky gates ranged between 45 and 100 nm, depending on the x-ray mask used. This variation from one mask to another was intentional.

The challenge in building the PRESTFET was to delineate two or three interdigitated Schottky gate fingers with minimum linewidth and pitch, connected to large gate pads. Narrow linewidth (i.e., short gate length) is important to maximize the tunneling probability; a minimum pitch is required to increase the separation of the quantized energy levels in the well. A large separation increases the temperature range over which resonant tunneling (RT) can be observed.

Figure 1 is a scanning electron micrograph of a triple-gate PRESTFET made by e-beam lithography. The gates were defined by exposing 100 nm thick PMMA, followed by Ti/Pt evaporation and liftoff. The source and drain Ohmic con-

Dose-rate effects in focused-ion-beam implantation of Si into GaAs

Henri J. Lezec, Christian R. Musil, and John Melngailis
Massachusetts Institute of Technology, Cambridge, Massachusetts 02139

Leonard J. Mahoney and John D. Woodhouse
Lincoln Laboratory, Massachusetts Institute of Technology, Lexington, Massachusetts 02173

(Received 2 December 1990; accepted 30 April 1991)

Ion current densities in focused-ion-beam (FIB) implantations are several orders of magnitude greater than those of conventional broad-beam implantations. The corresponding increase in dose rate during implantation is shown to affect parameters of interest in device fabrication. FIB and broad-beam Si implants into GaAs at energies from 70 to 280 keV and at doses from 3×10^{12} to 10^{14} cm^{-2} are characterized using secondary ion mass spectroscopy (SIMS) and Hall-effect measurements. Reduced straggle, decreased activation, and modified carrier profiles are observed for FIB implants, particularly at higher energies and doses. These effects are attributed to dose-rate-dependent lattice damage.

I. INTRODUCTION

Focused-ion-beam (FIB) implantation can perform unique functions which cannot be duplicated by conventional fabrication using broad-beam implantation.[1] In a mass-separated, scanned focused-ion-beam system, ions of common semiconductor dopants can be accelerated, focused down to a spot size on the order of 0.1 μm, and deflected under computer control to implant arbitrary patterns. The ability to vary the implant dose from pixel to pixel has permitted the fabrication of novel devices with lateral doping gradients[2] and novel circuits where the dose is varied from transistor to transistor.[3] Ion energy and ion species can be varied across a wafer as well, so the focused ion beam is ideally suited for prototyping applications.

Since the current density in a focused ion beam is typically many orders of magnitude higher than the current density in a conventional broad beam, one might expect differences in the electrical and structural properties of materials implanted to the same dose by the two different techniques. Such differences have been observed in both Si and GaAs. For example, measurements by Tamura *et al.*,[4,5] show that compared to conventional implantation, focused-beam implantation into Si results in increased lattice disorder.

On the other hand, measurements by Bamba *et al.*[6] using Raman scattering spectroscopy indicate a decrease in lattice disorder when GaAs is implanted with a 160 keV, focused ion beam of Si, compared to conventional broad-beam implantation at the same energy. Other reported characteristics include greater implant penetration range and straggle,[7] and higher post-anneal electrical activation.[6]

In the present study, the electrical characteristics and implant depth distribution of GaAs implanted with a focused ion beam of silicon are measured in the context of the fabrication and optimization of devices such as FIB Gunn diodes[2] and MESFETs with laterally graded implants. For purposes of comparison, implants with a conventional broad beam of silicon are also characterized.

Of particular interest are FIB implanted profiles and activation results which are significantly different from those of Bamba *et al.* even though the implants were performed at a comparable instantaneous ion-beam current density.

II. EXPERIMENT

The substrate material was obtained from M/A-COM and consisted of semi-insulating, liquid-encapsulated Czochralski (LEC) GaAs wafers that were sliced with the (100) axis either aligned with the surface normal (on-axis) or tilted 8° away (off-axis). The off-axis material was used to reduce channeling during focused ion-beam implantation. This was necessitated by the fact that the FIB sample stage cannot be tilted with respect to the incident beam.

Using a focused ion beam and a conventional broad beam, mass-28 silicon ions were implanted into each type of substrate at room temperature and at normal incidence. Energies ranged from 70 to 280 keV and doses ranged from 3×10^{12} to 1×10^{14} cm^{-2}.

The focused ion beam originated from a Au–Si liquid-metal ion source from which Si^+ and Si^{++} ions were extracted, separated, and focused using a three-lens, 150 kV column. A 40-pA, 0.25-μm diam beam was used, implying an ion-beam current density of 80 mA/cm^2. Implants were performed in a single pass during which the beam addressed pixels spaced apart by 0.1 μm, dwelling at each spot for 1.2–40 μs. Patterns suitable for SIMS profiling (750×750 μm squares) or Hall-effect measurements of the van der Pauw type (cloverleaf patterns with 60×60 μm central areas) were selectively implanted with respect to etched alignment marks.

The broad-beam implants employed a 5-mm diam beam and a beam current of 3 μA, implying an ion-beam current density of 15 μA/cm^2. Repeated scanning of the beam over the sample resulted in an average current density of 50 nA/cm^2. In this scheme, the total ion dose at each point was delivered in an intermittent fashion with approximately 500 to 16 400 beam pulses, each lasting 65 μs. The time between pulses was 19 ms.

During both FIB and broad-beam implantation, substrate heating was negligible, and beam collimation was within a few milliradians.

Following implantation, implanted atomic distribution and electrical activity were characterized by secondary-ion mass spectroscopy and Hall-effect measurements, respectively.

 0734-211X/91/052709-05$01.00

Appendix C

Lateral Straggle of Focused-Ion-Beam Implanted Be in GaAs

D. Vignaud[a], S. Etchin, K.S. Liao, C.R. Musil, D.A. Antoniadis and J. Melngailis

Research Laboratory of Electronics and
Department of Electrical Engineering and Computer Science
Massachusetts Institute of Technology
Cambridge, MA 02139

Abstract

The lateral distribution of focused-ion-beam implanted Be atoms in GaAs has been studied by measuring the electrical resistivity in grating structures. The gratings were implanted at 230 and 260 keV with periods from 0.04 μm to 3 μm oriented both parallel and perpendicular to the direction of current flow. In the parallel case an initially n-type conducting layer was converted to an insulating layer as the period of the unannealed implants was decreased. The resistivity was found to be modulated for grating periods even below 0.1 μm. In the perpendicular case the gratings were implanted into both on-axis and off-axis, semiinsulating GaAs between two p-type regions and rapid-thermal-annealed. The minimum half-width of an implanted line was found to be 140 nm in on-axis material. In off-axis material the width was 50 to 90 nm larger depending on dose. In all cases the width is smaller than the 450 nm straggle predicted by Monte-Carlo simulations.

To be published Appl. Phys. Lett. May 4, 1992

---

[a] On sabbatical leave from UA 234, Université des Sciences et Techniques de Lille Flandres Artois, Villeneuve d'Ascq France

IEEE ELECTRON DEVICE LETTERS, VOL. 9, NO. 9, SEPTEMBER 1988

A Tunable-Frequency Gunn Diode Fabricated by Focused Ion-Beam Implantation

HENRI J. LEZEC, KHALID ISMAIL, LEONARD J. MAHONEY, MARK I. SHEPARD, MEMBER, IEEE, DIMITRI A. ANTONIADIS, SENIOR MEMBER, IEEE, AND JOHN MELNGAILIS, SENIOR MEMBER, IEEE

Abstract—We report the fabrication of a planar Gunn diode in which the fundamental transit-time mode oscillation frequency can be tuned over the range 6–23 GHz by varying the dc bias across the device. The wide-band tunability is due to a linear doping concentration gradient between the contacts. This lateral doping profile was created by implanting the device with a focused beam of silicon ions and smoothly increasing the dose from contact to contact. A Gunn diode with a uniform active region, also fabricated with the focused ion beam, displays a relatively constant oscillation frequency in the same bias range.

I. Introduction

GaAs GUNN diodes are one of the most important solid-state sources of microwave power. Frequency tuning over a limited range is usually obtained in resonant circuits where a Gunn diode may operate in different modes of oscillation. Tuning is produced with an external device either mechanically, by varying the dimensions of a resonant cavity, or electronically using varactor diodes or ferrimagnetic material, particularly YIG spheres.

In 1967, Sandbank [1] and Shoji [2] proposed a Gunn diode with a transit-time mode frequency that is directly tunable with bias voltage. This effect can be obtained by smoothly increasing either the doping concentration or the cross section of the device from cathode to anode. Since a technology that allows precise control of lateral or vertical doping profiles was not available at the time, Gunn diodes with nonuniform cross sections were built instead. Tapered Gunn diodes [1], [2] and Gunn diodes with concentric electrodes [3]–[5] have displayed wide-band frequency tunability when connected to nonresonant resistive loads. For example, a planar Gunn diode with concentric electrodes was tunable with bias voltage over a range of 6.6–18 GHz [4].

With the recent advent of focused ion-beam technology, it becomes possible to implant planar structures with laterally graded doping profiles (for a review of the field of focused ion-beam technology see [6]). In our focused ion-beam system, ions of common semiconductor dopants can be accelerated up to 300 keV (if doubly ionized), focused down to a 0.1-μm spot size, and deflected under computer control for local implantation of arbitrary geometries. By modifying the exposure time per pixel as the beam is scanned along the surface of a wafer, smoothly varying lateral doping profiles can be achieved. We report the first use of this doping technique to build a planar tunable-frequency Gunn diode.

A vertical tunable-frequency Gunn diode could be built by grading the doping concentration of the active layer during epitaxial growth. The technology has already been demonstrated: using molecular beam epitaxy, Ondria and Ross [7] improved the operation of GaAs Gunn diodes by grading the active region doping profiles to minimize temperature gradients.

A distinct advantage of *planar* tunable-frequency Gunn diodes fabricated by focused ion-beam implantation is that they can be integrated directly into monolithic circuits. In addition, diodes with different lateral doping profiles and frequency versus bias characteristics can be defined on the same wafer or in the same circuit.

II. Principle of Operation

In a uniformly doped device, the fundamental transit-time frequency of oscillation is determined by the time it takes for the dipole domain to propagate from the cathode, where it nucleates, to the anode, where it discharges. The frequency is inversely proportional to this time and is relatively constant as a function of applied field.

In a device in which the doping level increases from cathode to anode, the applied electric field decreases from cathode to anode. The length over which the electric field exceeds the domain sustaining value $E_s \simeq 2$ kV/cm defines the length of repeated travel of the domain. When a domain reaches the point at which the field has dropped to E_s it dissolves, and a new domain is nucleated at the cathode. By varying the bias voltage, this point can be shifted across the sample, thus allowing control of the transit-time frequency [8]. When the bias across the device is increased, for example, the point at which the field has dropped to E_s moves toward the anode; the transit length and transit time increase and the frequency of oscillation decreases.

III. Fabrication

Semi-insulating GaAs was first implanted with a 140-keV, 25-pA, Si^{++} focused ion beam. The beam diameter was estimated to be about 0.15 μm from the resolution obtained while imaging a free-standing gold grating of 0.1-μm-wide lines. The planar implant geometry is shown in Fig. 1(a). The

Manuscript received May 11, 1988; revised July 8, 1988. This work was supported by DARPA/DOD under Contract MDA 903-85-C-0215 at M.I.T. and by the Department of the Air Force at Lincoln Laboratory.

H. J. Lezec, K. Ismail, M. I. Shepard, and D. A. Antoniadis are with the Department of Electrical Engineering and Computer Science, Massachusetts Institute of Technology, Cambridge, MA 02139.

L. J. Mahoney is with Lincoln Laboratory, Massachusetts Institute of Technology, Lexington, MA 02173.

J. Melngailis is with the Research Laboratory of Electronics, Massachusetts Institute of Technology, Cambridge, MA 02139.

IEEE Log Number 8823208.

0741-3106/88/0900-0476$01.00

Appendix E

Theory and Simulation of Ion-Implanted Laterally-Graded Gunn-Effect Diodes *

Christian R. Musil, Henri J. Lezec, Dimitri A. Antoniadis
and John Melngailis
Massachusetts Institute of Technology
Cambridge, MA 02139

Leonard J. Mahoney
Lincoln Laboratory
Massachusetts Institute of Technology
Lexington, MA 02173

Abstract

Planar Gunn-effect diodes with novel RF performance have been fabricated by implanting lateral doping gradients into GaAs using a Focused Ion Beam (FIB)[1]. As free-running tunable oscillators, these devices exhibit high frequency operation up to 42 GHz, wide tuning of 5 to 25 GHz, and power (~ -10 dBm) and impedance ($\mathrm{Re}\{Z\} \sim -50\ \Omega$) levels commensurate with direct MMIC integration. Applications of these diodes include their use as local swept-frequency sources for built-in test circuitry and miniature network analyzers.

An accurate understanding of domain nucleation and propagation in these highly-doped short-length diodes is not possible with conventional field-dependent transport theory. A sophisticated energy-dependent model based on the Boltzmann transport equation and incorporating non-stationary dynamic effects is used in this paper to simulate the underlying physical processes involved. Simulation results are presented and combined into a theory of tuning. Device operation is shown to be dominated by bias-dependent domain propagation length with renucleation driven by a gradient induced, current feedback effect. Gunn diodes with tailored frequency-versus-voltage characteristics are discussed in context of theory and simulation. In addition, the effects of dopant variation in depth is also discussed.

*Work supported by DARPA/ARO contract no. DAAL-88-K-0108 and by the Department of the Air Force at Lincoln Laboratory.

[1] A. Chu, et al, *IEEE MTT-S Digest*, 1179 (1991).

Appendix F

Performance and Applications of Novel Oscillators utilizing Focused Ion Beam Implanted Gunn-Effect Devices+

A. Chu*, L. Chu, W. Macropoulos, K. Khair, R. Patel
M/A COM Integrated Subsystems Division, Chelmsford, MA 01824

M. Cordaro
Universidade de Sao Paulo, Sao Paulo - SP - Brazil

H.J. Lezec, J. Melngailis
Massachusetts Institute of Technology
Cambridge, MA 02139

L.J. Mahoney
Lincoln Laboratory Massachusetts Institute of Technology
Cambridge, MA 02173

ABSTRACT

The RF performance of novel and compact voltage controlled (VCO), injection locked (ILO) and dielectric resonator oscillators (DRO) utilizing tunable Focused Ion Beam Implanted (FIBI) Gunn diodes will be reported for the first time. Frequency tuning from 5 to 25 GHz is the widest band achieved with a single oscillator by varying the bias voltage across the FIBI Gunn device.

+Work at MIT supported by DARPA/ARO contract no. DAAL03-8-K-0108 and by the Department of the Air Force at Lincoln Laboratory.

*A. Chu is presently at MITRE Corporation, Bedford, MA 01730

To be presented at 1991 IEEE MTT-S Intrn. Microwave Symp, June 11-14, 1991 Boston, MA.
Also in IEEE MTT-S Digest, 1179

Increase in silicon charge coupled devices speed with focused ion beam implanted channels

J. E. Murguia, M. I. Shepard, and J. Melngailis
Research Laboratory of Electronics, Massachusetts Institute of Technology, Cambridge, Massachusetts 02139

A. L. Lattes and S. C. Munroe[a)]
Lincoln Laboratory Massachusetts Institute of Technology, Lexington, Massachusetts 02173

(Received 2 December 1990; accepted 30 April 1991)

The clocking frequency of long channel CCDs is limited by the time taken to transfer charge from one well to the next. The bulk of the charge transfers rapidly by Coulomb repulsion but residual charge has to transfer by thermal diffusion, which is a slow process. If the *n*-type dopant density has a gradient in the direction of current flow, a built-in electric field is created, speeding up the charge transfer process. The focused ion beam system is uniquely suited to implant such a gradient of doping and has been used to implant buried-channel CCDs with 26-μm-long storage gates. The devices built to demonstrate this concept were shallow-buried-channel CCDs driven by 2-phase 5-V clocks. Arsenic ions were implanted at an energy of 220 keV and a gradient of doping increasing from 0 to 1.5×10^{11} ions/cm^2 was superimposed on a uniform phosphorus implant. The challenge here was to get a *low*, monotonically increasing implant dose. Defocusing of the 25-pA As^{++} beam to a diameter of ~1 μm was found to be necessary. The maximum operating (clocking) frequency of the graded-implant devices was 41 MHz compared to a maximum frequency of 2.5 MHz for the same devices with uniformly doped channels. Such long-channel CCDs are of interest in 2-dimensional imaging applications and signal processing applications where high well charge capacity is needed without compromising speed or charge transfer efficiency.

I. INTRODUCTION

Charge-coupled devices (CCDs) are composed of a series of MOS capacitors (also called wells or channels) operated in deep depletion.[1] Appropriate clocking voltages are used to transfer charge between adjacent wells, which can number in the hundreds. CCDs are used in signal processing and imaging. The key parameters which characterize the operation of a CCD are the maximum clocking frequency, the charge transfer efficiency, and the charge handling capacity. Increasing the length of the channels of a CCD will increase the charge handling capacity at the expense of clocking frequency. CCD infrared imagers, in particular, typically operate with pixels (in effect, channels) of dimensions from 20 to 50 μm.[2] When a clock pulse is applied and the electrons in a given well are presented with an adjacent well at lower potential, most of them rapidly transfer by Coulomb repulsion. This transfer lowers the driving potential, and the residual charge has to transfer by diffusion and drift due to fringing fields. The average time for a single electron to travel 26 μm in Si, for example, is about 200 ns. (Ref. 3). Thus the maximum clocking frequency of CCDs with 26-μm channel length is expected to be below 5 MHz (see Fig. 1).

If a gradient of *n*-type dopant is created in the well in the direction of current flow, an electric field results which is predicted to speed up the transfer of these electrons by a factor of 25. (Ref. 3). Nonuniformly implanted doping profiles have been used in the early 1970's to achieve unidirectional operation in two-phase CCDs,[9,10] and gradients have been suggested for increased clocking speed.[11] However, no easy method existed for implanting such gradients. The focused ion beam is the ideal tool for implanting the desired doping gradient since the alloy sources which emit the dopants of Si have been developed.[4,5] In this paper we will describe the implantation of CCDs with doping gradients and briefly mention the improvement in performance achieved. The design, electrical characteristics, and testing will be described elsewhere.[3]

II. DEVICE FABRICATION

The CCDs fabricated were of the buried-channel type, in which the minimum potential for electrons is away from the Si–SiO_2 interface.[1] The focused ion beam gradient implant served to slope the minimum potential further downward in the direction of current flow as shown schematically in Fig. 1.

The structure at this stage is shown schematically in Fig. 2 in cross section. The phosphorus implant was carried out in two steps using the barrier gate as the mask for the second step. This resulted in a barrier potential on the left-hand side of each well as shown schematically in Fig. 1 (top). The focused ion beam implant was carried out at 220 keV with As^{++} ions to produce a gradient of doping as shown (shaded) at the bottom of Fig. 2 over the 26-μm length of the channels. The desired gradient calculated by simulations[3] was a uniform ramp from 0 to 1.5×10^{11} ions/cm^2 over 26 μm. The expected depth profiles of the As implant superimposed on the phosphorus implant are shown in Fig. 3.

This very low dose presented a special challenge. The minimum dwell time of our focused ion beam system is 200 ns. Thus if the beam is 0.1 μm in diameter with 20 pA of current, the minimum dose that can be delivered is 1.5×10^{11} ions/cm^2. If the beam current were further reduced by reducing the beam defining aperture, the ability to see align-

 0734-211X/91/052714-04$01.00

Appendix H

Improved Drift in Two-Phase, Long-Channel, Shallow-Buried-Channel CCD's with Longitudinally Nonuniform Storage-Gate Implants

A. L. Lattes, S. C. Munroe,* M. M. Seaver
Lincoln Laboratory, Massachusetts Institute of Technology
Lexington, Massachusetts 02173-9108

J. E. Murguia†
Research Laboratory of Electronics, Department of Electrical Engineering
and Computer Science, Massachusetts Institute of Technology
Cambridge, Massachusetts 02139

J. Melngailis
Lincoln Laboratory, Massachusetts Institute of Technology
Lexington, Massachusetts 02173-9108
Research Laboratory of Electronics, Department of Electrical Engineering
and Computer Science, Massachusetts Institute of Technology
Cambridge, Massachusetts 02139

Abstract

The charge transfer efficiency (CTE) of two-phase charge-coupled devices (CCD's) has been significantly improved by a built-in potential gradient in the storage wells. The potential gradient was generated by a nonuniform channel doping parallel to the surface. Shallow-buried-channel CCD's operating with two-phase 5-V clocks and having storage gates 26 μm long were designed, fabricated and tested. Two-dimensional computer simulations predict that the fringing fields in these structures should be negligibly small near the center of the wells, while the built-in drift fields generated by the nonuniform implants can be relatively large (> 30 V/cm). Experimental results, both at room temperature and at 77 K, show that the resulting drift field improves the CTE by more than an order of magnitude.

*Current address: Analog Devices, Wilmington, MA.
†Current address: Lincoln Laboratory, Massachusetts Institute of Technology.

Submitted to IEEE Transactions on El. Devices.